BioMed Research Journal
BMRJ, 6(1): 491-500
www.scitcentral.com

ISSN: 2578-8892

Original Research Article: Open Access

# Effect of Low Calcination Temperature of Nickel Ferrite Nanoparticles on Magnetic, Optical and Anti-Algal Properties

**Praveena MG[1,2*], Kala MS[2], Viji C[1], Shyam Kumar S[3] and Mohammed EM[1]**

*[*1]Department of Physics, Maharaja's College, Ernakulam, Kerala, India*

*[*2]Department of Physics, St. Teresa's College, Ernakulam, Kerala, India*

*[3]Department of Botany, Maharaja's College, Ernakulam, Kerala, India.*

*Received October 05, 2021; Revised October 15, 2021; Accepted October 28, 2021*

## ABSTRACT

Nickel ferrite ($NiFe_2O_4$) nanoparticles were synthesized using the sol-gel auto combustion method, and the powdered samples were calcined at two temperatures, 100°C and 200°C. The structure of nickel ferrite nanoparticles was determined using X-ray diffraction (XRD) patterns. The nickel ferrite nanoparticle size was calculated using the Debye-Scherrer formula and was found to be 15.53 nm and 17.14 nm for 100°C and 200°C. Field Emission Scanning Electron Microscopic (FESEM) analysis reveals that the samples exhibit spherical morphology with crystalline in nature and also shows some agglomeration. The phase formation of nickel ferrite nanoparticles was further confirmed from the energy dispersive x-ray (EDAX) spectra which shows strong peaks for the existence of all the elements in it. The work investigates the magnetic properties of the samples and both the samples exhibits ferromagnetic behavior. The optical band gap obtained for the samples are 2.5 and 2.6 eV for $N_1$ and $N_2$ samples. The antimicrobial activity especially the anti-algal effect of $NiFe_2O_4$ nanoparticles on freshwater microalgae Chlorella pyrenoidosa in a dose-dependent manner is also reported.

**Keywords**: Chlorella pyrenoidosa, Nickel ferrite, Magnetic characteristics, Optical band gap

## INTRODUCTION

The novel properties of nanostructured materials have received much attention in the scientific community. Due to their large surface area, unusual adsorptive properties, surface defects, and high diffusivity, there has been a growing interest in the synthesis of multifunctional metal oxides in recent decades [1-10]. The magnetic ferrite nanoparticles are used for hyperthermia for cancer treatment, ferrofluid, magnetic drug delivery [11-14]. The physical properties of ferrites are tuned by the chemical composition and method of processing. Spinel ferrites are a class of metal oxides generally conveyed by the stoichiometric formula $AFe_2O_4$, where A is the divalent metal cations such as Co, Mg, Ni, and Zn. Nickel ferrite ($NiFe_2O_4$) nanoparticle found very much interest among the spinel ferrites due to their multifunctional properties and are widely used for applications like magnetic drug delivery, microwave devices, and magnetic resonance imaging [15-19]. Nickel ferrite nanoparticles have an inverse spinel structure with a face-centered cubic crystal structure. Production of ferrite nanoparticles has increased in recent years due to their broad range of application in technical and biomedical fields; thus, many nanoparticles may reach the environments internally or externally, where their purpose and behavior are largely unknown [20,21]. Nanoparticles show a different toxicity profile than their bulk counterparts due to their potential to interact more effectively with biological systems due to their nano size and massive surface area [22-27]. In recent years, algae have been widely used in ecological risk assessments to evaluate the impacts of metal, herbicide, and other xenobiotic contamination and bioavailability in aquatic systems. The main reason for their use is their sensitivity to many contaminants at environmentally relevant concentrations [28]. The soft magnetic and n-type semiconducting nickel ferrite can be synthesized by various physical and chemical methods like mechanical mixing, sol-gel, coprecipitation, ceramic method, hydrothermal etc [29-34]. The ferrites' properties are influenced by microstructure and composition, which are very sensitive to the processing

**Corresponding author:** Praveena M G Department of Physics, Maharaja's College, Ernakulam College, 682011, Kerala, India, Tel: 9747725527; E-mail: pravigvr05@gmail.com, emmohammed_2005@yahoo.com

**Citation:** Praveena MG, Kala MS, Viji C, Kumar SS & Mohammed EM. (2022) Effect of Low Calcination Temperature of Nickel Ferrite Nanoparticles on Magnetic, Optical and Anti-Algal Properties. BioMed Res J, 6(1): 491-500.

techniques. Reasonable stoichiometric control and synthesize of ultrafine particles with a narrow size distribution with less processing time are the advantage of the sol-gel method [35]. The present research work aims to employ a conventional sol-gel auto combustion method to synthesize the $NiFe_2O_4$ nanoparticles and to check their anti-algal effect. The role of particle size is also investigated by calcining the nanoparticle at different temperature. The antimicrobial property is specifically dependent to the nanoparticles size. This is because they possess greater capability to reach in to the cell membrane and they have large surface area particularly in suspension. So that the $NiFe_2O_4$ nanoparticles were calcined at two temperatures, 100ºC and 200ºC, respectively. Characterized the samples using powder X-ray diffraction and FESEM-EDAX, magnetic and optical properties of the samples were investigated. We explore the effect of the nanoparticles for microalgae Chlorella pyrenoidosa. And also investigated the influence of particle size of nickel ferrite nanoparticle on the antialgal efficiency.

## EXPERIMENTAL DETAILS

### Synthesis of $NiFe_2O_4$ nanoparticle

For the preparation of nanoparticles, stoichiometric ratios of AR grade Ferric nitrate ($Fe(NO3)_3.9H_2O$) and Nickel nitrate ($Ni(NO_3)_2.6H_2O$) were dissolved in a minimum amount of ethylene glycol at room temperature. After that, the solution is heated to 60°C to form a wet gel. The gel was then dried at 120°C for 2 h, after which it self-ignited to form $NiFe_2O_4$ powder. The combustion of the gel can be thought of as a thermally induced redox reaction in which ethylene glycol acts as a reducing agent and the nitrate ion acts as an oxidant. The nitrate ion provides an in situ oxidizing atmosphere for the decomposition of the organic component. The obtained product was then finely ground. The powder was separated into two parts and calcined at two different temperatures 100°C and 200°C, for 2 h in a muffle furnace.

### Culturing of the algae

Experiments were carried out at the Marine Botany Laboratory, School of Marine Sciences, CUSAT, with freshwater green algae belonging to the division Chlorophyta, Chlorella pyrenoidosa. The exponentially growing Chlorella pyrenoidosa with a cell density of 6 x 104 cells/ml was taken 15 ml, and it was inoculated into a 150ml Walnes medium contained in a 250ml Erlenmeyer flasks in the absence and presence of the test substance. The culture without the content of nickel ferrite was taken as the control. $NiFe_2O_4$ calcined at different temperatures were added to the test culture. The cultures were incubated at the optimum conditions of growth for eight days. The incubation of the culture was done using two cold white fluorescent light of 1250 lux each for a light/dark period of 12:12 h. Cultures were maintained at room temperature ($30 \pm 2^0$C).

### Algal growth inhibition study

The algal growth inhibition analysis was carried out by measuring algal chlorophyll content and cell count every 48 h. Algal cell density was measured using a Neubauer Hemocytometer in cell numbers (algal cell/ml). Cell count investigated the effect of nickel ferrite annealing temperature on Chlorophyll for 8 days with a regular interval of 48h. The specific growth rate was calculated using the below equation (1) [36].

$$\mu = \frac{L_n N_t - L_n N_0}{t_n} \quad (1)$$

$N_t$ is the measured final cell density, $N_0$ the initial cell density (6 x 104 cells/ml), $t_n$ is the incubation period (in days).

### Characterization of $NiFe_2O_4$ nanoparticles

The phase composition and crystal structure $NiFe_2O_4$ nanoparticles were identified using the XRD (X-Ray Diffraction) analysis at room temperature for a range of 2 theta values 20° to 80° on using Rigaku Mini Flex 600 equipped with Cu Kα radiation (λ = 1.5406 Å). The prepared nanoparticles' structural morphology was studied using the FESEM (Field Emission Scanning Electron Microscopy) analysis. FESEM analysis for the $NiFe_2O_4$ was recorded using a ZEISS sigma microscope attached with EDAX set up. The presence of various elements in the samples was investigated from the EDAX spectrum. The optical properties exhibited by the $NiFe_2O_4$ nanoparticles was analyzed from UV-Vis (Diffusion Reflectance Spectrum) spectrum. The prepared nanoparticles' magnetic properties were studied from the VSM (Vibrating Sample Magnetometer) analysis result. The powder samples were used for the analysis.

## RESULTS AND DISCUSSION

### X-Ray Diffraction Analysis

The diffraction pattern reveals the cubic spinel structure of the prepared nickel ferrite nanoparticles. The obtained XRD diffractogram for the nickel ferrite nanoparticles calcined at two temperatures (100 °C and 200 °C) is shown in **(Figure 1)** Sharp well defined and intense peaks were observed for the synthesized samples. No impurity peaks confirm a single-phase nickel ferrite nanoparticles formation, thereby ensuring the synthesized samples' phase purity. The diffraction peak pattern was indexed using the standard JCPDS card no-074-2081. The mean crystallite sizes for the samples were calculated from the X-ray line broadening using the Debye–Scherer equation given in equation (2).

$$D = (0.9*\lambda) / (\beta\cos\theta) \quad (2)$$

Where λ represents the X-ray wavelength's wavelength, β is the full-width half maximum (FWHM) of the diffraction pattern, and θ is Bragg's angle. The average particle size obtained for the two prepared nickel ferrite nanoparticles is

tabulated in **(Table 1)**. The average nanoparticle size is 15.53 nm and 17.14 nm for 100 °C and 200 °C calcined nickel ferrite. To compare the value of the lattice parameters obtained for the nickel ferrite sample calcined at two different temperatures, the lattice parameter a was also calculated using the relation (3).

$$a = d_{(hkl)} / (h^2+k^2+l^2)^{1/2} \quad (3)$$

The lattice constant is almost constant and shows only minor variations with sintering temperature, as shown in the table. However, the size of the nanoparticles increases with calcination temperature. The prepared nickel ferrite samples with a cubic structure have Fd-3m space group.

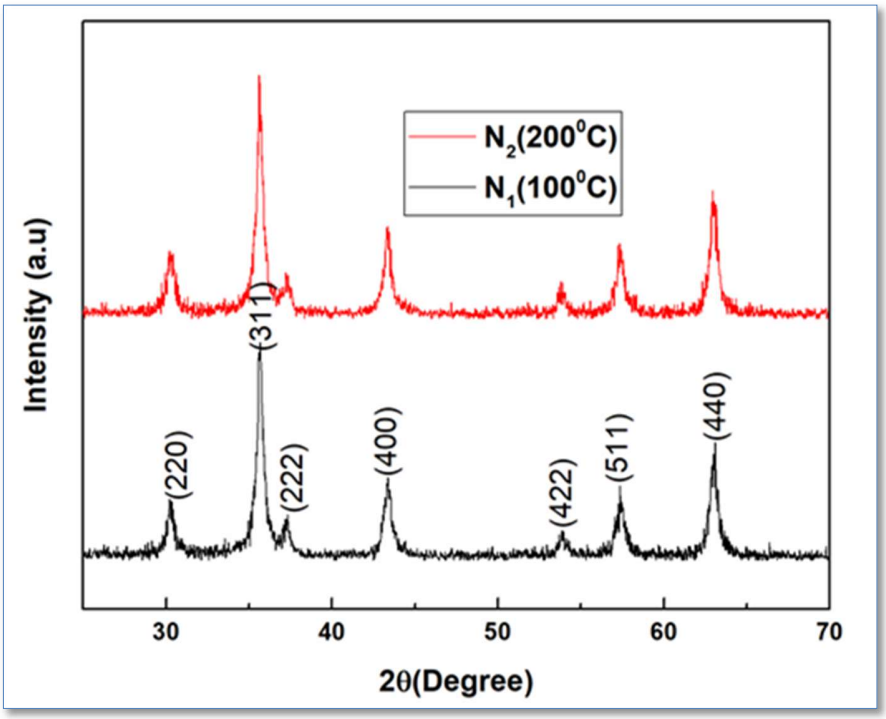


**Figure 1.** XRD diffractogram for $NiFe_2O_4$ at 100°C ($N_1$) and $NiFe_2O_4$ at 200°C ($N_2$).

**Table 1.** List of particle size and constant lattice values obtained for $NiFe_2O_4$ at 100°C ($N_1$) and $NiFe_2O_4$ at 200°C ($N_2$)

| 2θ ($N_1$) | Particle size D(nm) | Lattice Parameter a (Å) | 2θ ($N_2$) | Particle size D(nm) | Lattice Parameter a (Å) |
|---|---|---|---|---|---|
| 30.25 | 16.8077 | 8.3565 | 30.22 | 19.1516 | 8.3383 |
| 35.64 | 14.1544 | 8.3547 | 35.69 | 16.0621 | 8.3411 |
| 43.38 | 16.4544 | 8.4342 | 43.36 | 18.2036 | 8.3434 |

**Field Emission Scanning Electron Microscopy analysis**

The morphology of the prepared $NiFe_2O_4$ nanoparticles was analyzed from the FESEM micrographs, shown in **(Figures 2 & 4)**. FESEM micrograph illustrates the micrometrical aggregation of tiny spherical nanoparticles. The presence of high-density agglomeration suggests the presence of pore-free crystallites on the surface. The nanoparticles agglomerate and expand into larger assemblies due to their high surface energies.

EDAX analysis was used to look at the various elements present in the prepared samples. In both the samples, the spectrum displays strong peaks corresponding to O, Fe, and Ni, which implies the samples' phase purity. The atomic weight percentage of each element in the nickel ferrite sample calcined at 100 °C is given in **(Figures 3 & 5)** The homogenous distribution of iron, nickel and oxygen in the ferrite nanoparticles is confirmed from EDAX mapping, and it is shown in **(Figures 2d & 4d)**. The stoichiometric formula of nickel ferrite requires Ni, Fe, and O's ratio as 1:2:4. The presence of carbon in the spectrum is due to the carbon coating over the grid to place the sample for the measurements. We could see that prepared samples meet the requirements or the expected composition and elements from the results. Hence, the chemical composition requirement of the $NiFe_2O_4$ is in good agreement with the results obtained by our study.

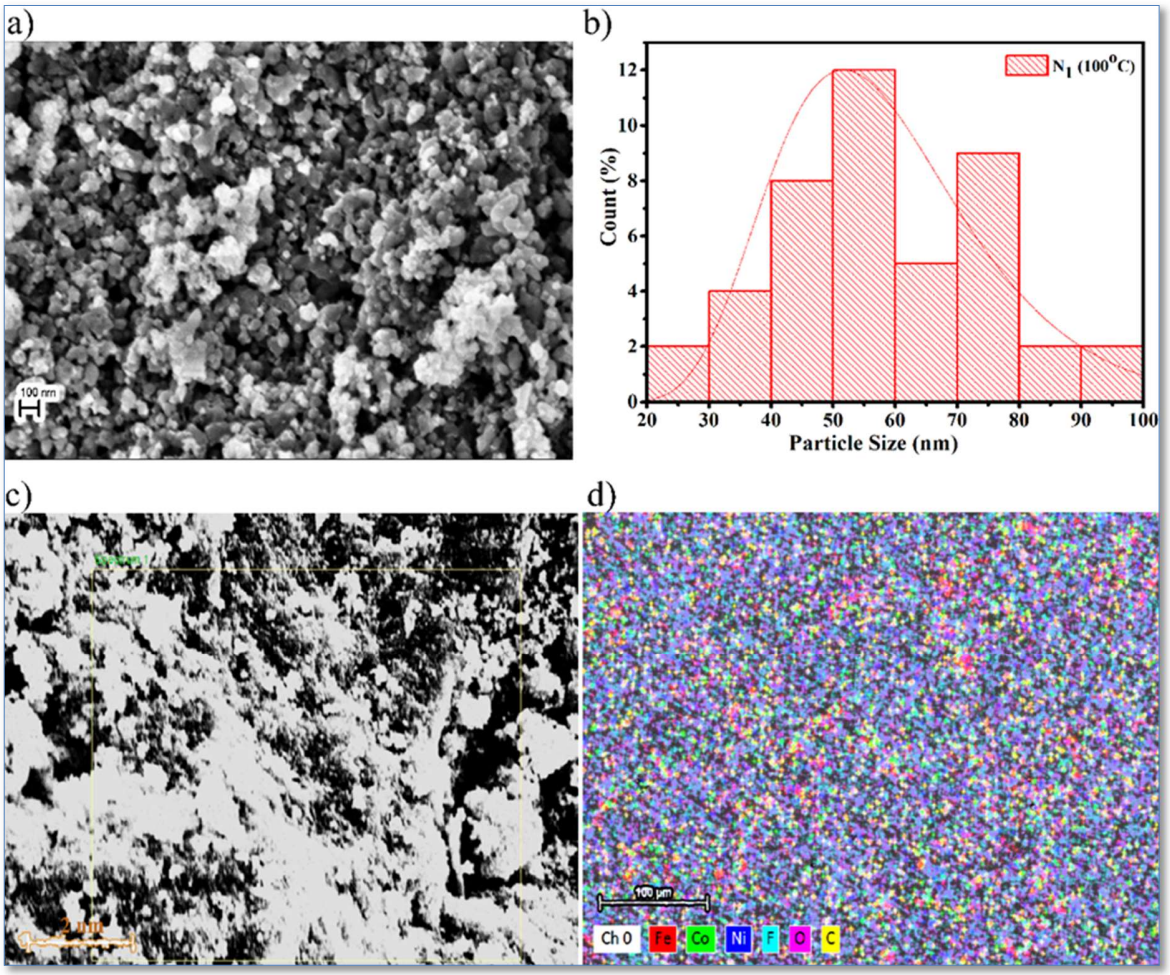


**Figure 2.** a) and b) represents the FESEM micrograph and histogram of particle distribution c) and d) corresponds to the EDAX image mapping for $NiFe_2O_4$ at 100°C ($N_1$).

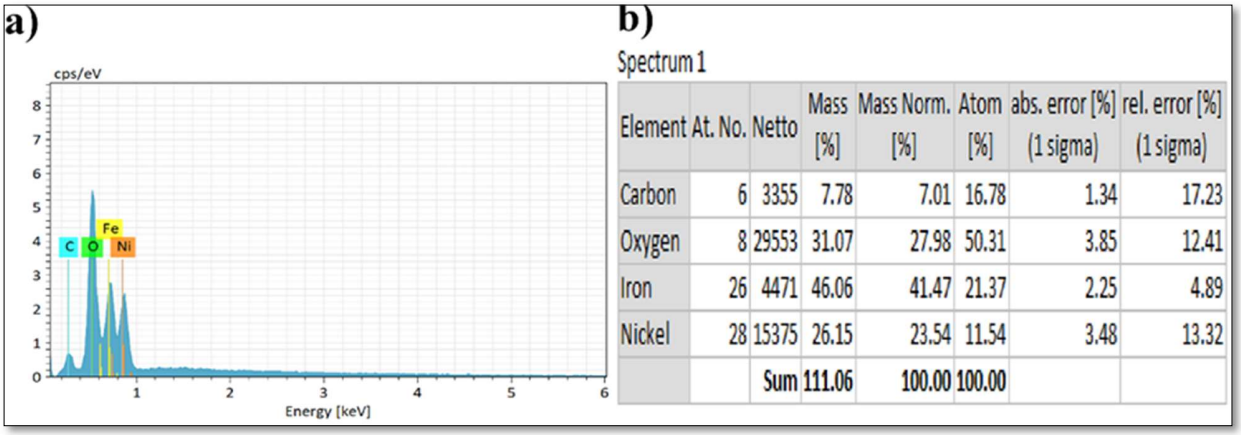


b)

Spectrum 1

| Element | At. No. | Netto | Mass [%] | Mass Norm. [%] | Atom [%] | abs. error [%] (1 sigma) | rel. error [%] (1 sigma) |
|---|---|---|---|---|---|---|---|
| Carbon | 6 | 3355 | 7.78 | 7.01 | 16.78 | 1.34 | 17.23 |
| Oxygen | 8 | 29553 | 31.07 | 27.98 | 50.31 | 3.85 | 12.41 |
| Iron | 26 | 4471 | 46.06 | 41.47 | 21.37 | 2.25 | 4.89 |
| Nickel | 28 | 15375 | 26.15 | 23.54 | 11.54 | 3.48 | 13.32 |
| | | Sum | 111.06 | 100.00 | 100.00 | | |

**Figure 3.** a) the EDAX spectrum and b) is the table showing the atomic weight percentage of each element in the $NiFe_2O_4$ at 100°C ($N_1$) sample.

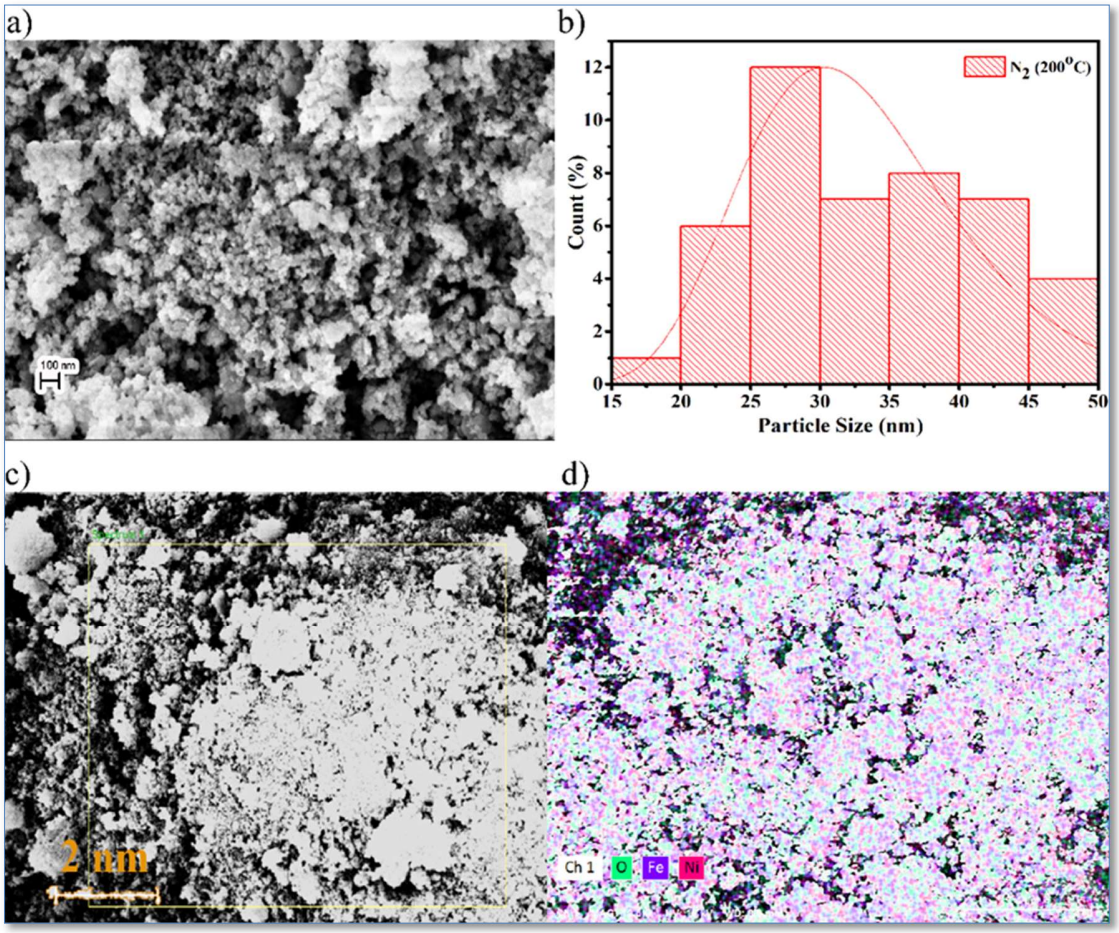


**Figure 4.** a) and b) represents the FESEM micrograph and histogram of particle distribution c) and d) corresponds to the EDAX image mapping for $NiFe_2O_4$ at 200°C ($N_2$).

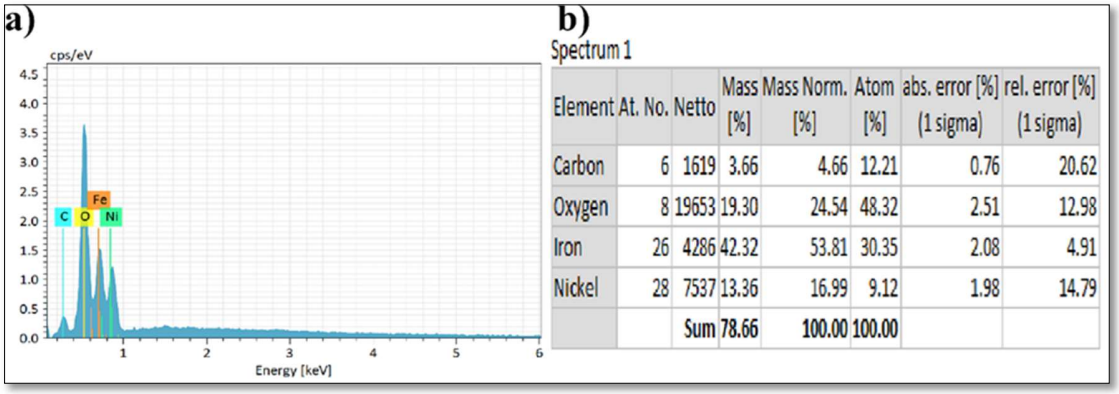


| Element | At. No. | Netto | Mass [%] | Mass Norm. [%] | Atom [%] | abs. error [%] (1 sigma) | rel. error [%] (1 sigma) |
|---|---|---|---|---|---|---|---|
| Carbon | 6 | 1619 | 3.66 | 4.66 | 12.21 | 0.76 | 20.62 |
| Oxygen | 8 | 19653 | 19.30 | 24.54 | 48.32 | 2.51 | 12.98 |
| Iron | 26 | 4286 | 42.32 | 53.81 | 30.35 | 2.08 | 4.91 |
| Nickel | 28 | 7537 | 13.36 | 16.99 | 9.12 | 1.98 | 14.79 |
| | | Sum | 78.66 | 100.00 | 100.00 | | |

**Figure 5.** a) the EDAX spectrum and b) is the table showing the atomic weight percentage of each element in the $NiFe_2O_4$ at 200°C ($N_2$) sample.

**The magnetic properties analysis**

The synthesized nickel ferrite nanoparticles' magnetic characteristics are studied using the VSM measurements with an external applied magnetic field ranging from - 25 kOe to +25 kOe. The room temperature magnetic hysteresis loop is shown in **(Figure 6)**. The values of magnetic parameters remanence, coercivity, saturation magnetization and magnetic squareness ratio were noted and listed in **(Table 2)**. It could be noted that a soft ferromagnetic nature of nickel ferrite was observed from the M-H loop. The magnetic parameters show a decreasing value with an

increase in calcination temperature and connected to the increasing grain size. The decrease in the value of coercivity for the prepared nickel ferrite nanoparticles compared bulk can be interpreted by considering the reduced porosity and increased crystallite size. The nanoparticle's saturation magnetization value is in the range of 41-45 emu/g, which is small compared to bulk nickel ferrite (55 emu/g) [37-39]. The magnetic squareness ratio value at and above 0.5 corresponds to materials having single magnetic domain size and the value below 0.5 implies to materials with the multi domain structure. So according to that the prepared nickel ferrite nanoparticle exhibits multi domain structure with orientation changes with the applied magnetic field facilitated by the movement of domain walls [40-43].

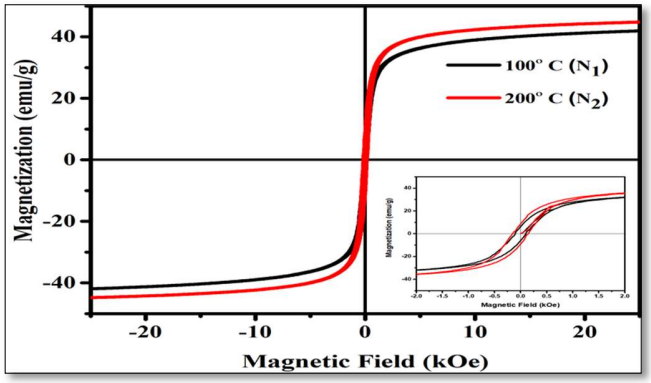


**Figure 6.** The M-H hysteresis loop showing the variation of magnetization value with applied magnetic field for the synthesized $NiFe_2O_4$ at 100°C ($N_1$) and $NiFe_2O_4$ at 200°C ($N_2$).

**Table 2.** The variation of magnetic order parameters for the nickel ferrite nanoparticles.

| Calcination temperature (ºC) | Size of nickel ferrite nanoparticle (nm) | Remanence $M_r$ (emu/g) | Saturation Magnetization $M_s$ (emu/g) | Coercivity $H_c$ (Oe) | Squareness Ratio ($M_r/M_s$) |
|---|---|---|---|---|---|
| 100 | 15.53 | 6.39 | 41.8 | 101 | 0.152 |
| 200 | 17.14 | 8.6 | 44.7 | 151 | 0.192 |

**Linear optical Property analysis**

The optical properties of the prepared nanoparticles were explored using UV-vis diffuse reflectance spectroscopy. **(Figure 7a)** displays the obtained reflectance spectra of Kebelka Munk function vs photon energy (hν). To determine the optical band gap, the Tauc plot is used and is shown in **(Figures 7b & 7c)**. The Kebelka Munk function using the reflectance data was used for the calculation of bandgap energy.

$$F(R) = \frac{(1-R)^2}{2R} \qquad (4)$$

Where F(R) is the Kubelka - Munk function and R is the reflectance value. $(F(R)h\nu)^2$ versus hv is plotted by considering the direct transition model for the nickel ferrite nanoparticles. The nickel ferrite sample's calculated band gap energy value is 2.5 and 2.6 eV for $N_1$ and $N_2$ samples, respectively. The nanoparticles' bandgap energy can be affected by the calcination temperature and crystallite size [44-48]. So that a slight variation is observed in the bandgap energy value is observed.

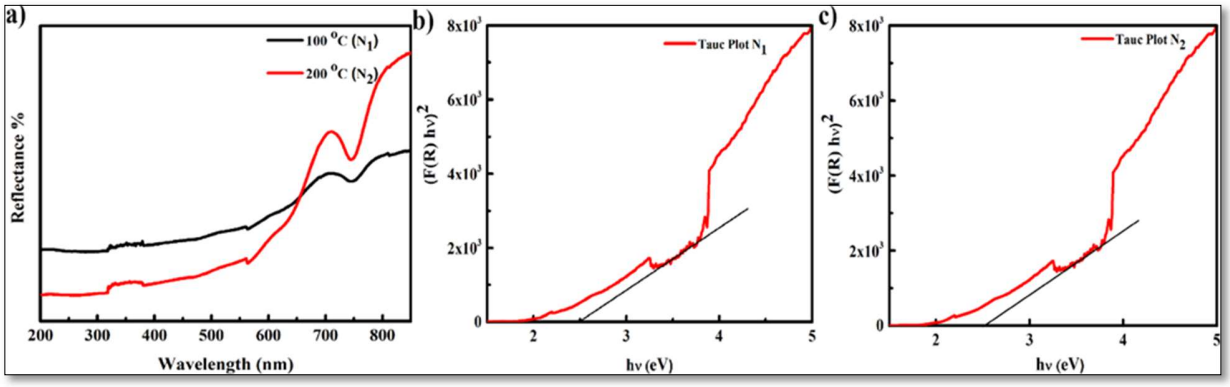


**Figure 7.** UV- Vis DRS spectra of a) $NiFe_2O_4$ at 100°C ($N_1$) and $NiFe_2O_4$ at 200°C ($N_2$). b) and c) Tau'c Plot for $N_1$ and $N_2$.

**Photosynthesis pigment analysis**

The effect of nickel ferrite nanoparticles on pigment content as a measure of algal growth was investigated. The (**Figures 8a & 8b)** shows the variation of growth of Chlorophyll-a for a time gap of 48h for the control (without nanoparticles) and different calcination temperature of $NiFe_2O_4$.

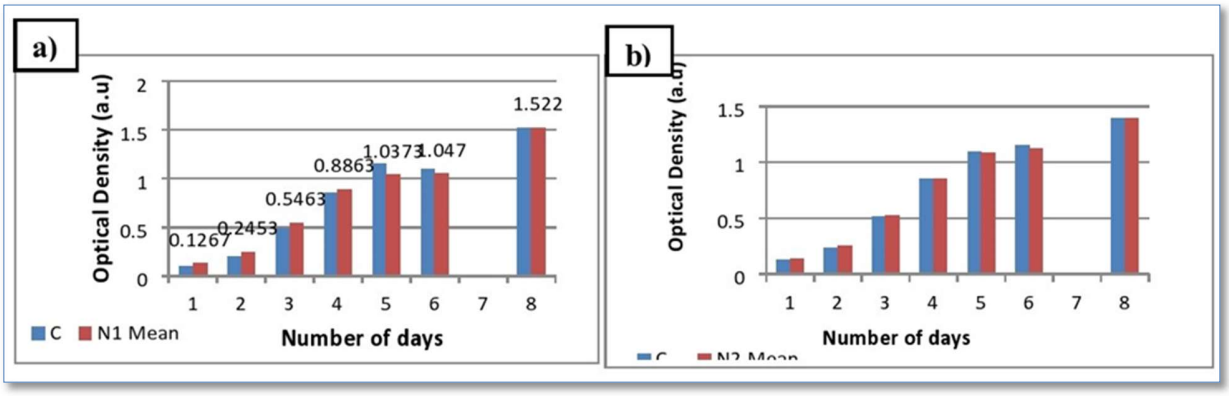


**Figure 8**. a) and b) represents the variation of Chlorophyll-a growth for a time gap of 48h for the control (without nanoparticles) and $NiFe_2O_4$ calcined at two temperatures.

Chlorophyll a content shown a significant reduction in growth with exposure to $NiFe_2O_4$ nanoparticles in contrast to the control (untreated) value, which is given in **(Table 3)**. The increase in the calcination temperature of nanoparticles shows an impact on the growth rate of the algae Chlorophyll-a, and it gets decreased. The cell density decreases as the calcination temperature rises, indicating that the calcination temperature of nickel ferrite has an inhibitory effect. The abnormal behavior of nickel ferrite on Chlorella pyrenoidosa may be due to the fact that, while nickel and iron are important micronutrients for algal metabolism, they can also be toxic and inhibit metabolic processes when used in amounts higher than the optimal level [49-53]. This observed variability in algal toxicity may be due to a variety of factors. Abiotic factors such as the composition of culture and test medium may have a major effect on the organism's tolerance level [54].

**Table 3.** The growth rate observed for control and the nickel ferrite nanoparticles.

| Sample code | Growth rate |
|---|---|
| C (control) | 0.078048 |
| $N_1$ | 0.077117 |
| $N_2$ | 0.071808 |

## CONCLUSION

This study focused on the dielectric properties and antialgal efficiency of the prepared nickel ferrite nanoparticles towards the green algae *Chlorella pyrenoidosa* for the first time. Nickel ferrite ($NiFe_2O_4$) nanoparticles with two different particle sizes were synthesized by the sol-gel auto combustion method. The phase purity and cubic spinel structure of nickel ferrite were established from the XRD pattern. The FESEM analysis of the nanoparticles reveals spherical-shaped particle with some agglomerations. The elemental composition of the samples was verified from EDAX analysis. The optical band gap of 2.5 and 2.6 eV for $N_1$ and $N_2$ samples was calculated from UV measurement. The nanoparticles behave like soft ferrites with saturation magnetization in the range of 41-45 emu/g. Our results indicate that $NiFe_2O_4$ calcined at 200°C shows a stimulatory effect on *Chlorella pyrenoidosa,* but the sample calcined at 100°C inhibits the growth. This dual influence of calcination temperature of nickel ferrite on the algal growth can be interpreted as when the usage of nickel ferrite nanoparticles in amounts higher than the optimal level can be toxic and inhibit metabolic processes.

## ACKNOWLEDGEMENTS

The authors gratefully acknowledge the Kerala State Council for Science, Technology and Environment (KSCSTE), Kerala, India, for the financial support. We thank the Head of the Department of Physics and the Principal, Maharaja's College, Ernakulam. The authors thank Dr Swapna S.Nair, Central University of Kerala, Kasaragod, for the VSM measurements.

## REFERENCES

1. Almessiere MA, Slimani Y, Güner S, Baykal A, Ercan I, et al. (2019) Effect of dysprosium substitution on magnetic and structural properties of NiFe2O4 nanoparticles. J Rare Earth 37: 871-878.
2. Korkmaz AD, Güner S, Slimani Y, Gungunes H, Amir MD, et al. (2019) Microstructural, Optical, and Magnetic Properties of Vanadium-Substituted Nickel Spinel Nanoferrites. J Supercond Nov Magn 32: 1057-1065.
3. Slimani Y, Almessiere MA, Güner S, Tashkandi NA, Baykal A, et al. (2019) Calcination effect on the

magneto-optical properties of vanadium substituted NiFe2O4 nanoferrites. J Mater Sci Mater Electron 30: 9143-9154.

4. Almessiere MA, Ünal B, Slimani Y, Korkmaz AD, Baykal A, et al. (2019) Electrical properties of La3+ and Y3+ ions substituted Ni0.3Cu0.3Zn0.4Fe2O4 nanospinel ferrites. Results Phys 15: 102755.
5. Nawaz M, Almessiere MA, Almofty SA, Gungunes CD, Slimani Y, et al. (2019) Exploration of catalytic and cytotoxicity activities of CaxMgxNi1-2xFe2O4 nanoparticles. J Photochem Photobiol B Biol 196: 111506.
6. Almessiere AM, Slimani Y, Sertkol M, Nawaz M, Sadaqat A, et al. (2019) Effect of Nb3+ Substitution on the Structural, Magnetic, and Optical Properties of Co0.5Ni0.5Fe2O4 Nanoparticles. J Nanomater 9: 430.
7. Yasin G, Junaid M, Uzair M, Abubaker M, Qamar W, et al. (2020) Revealing the erosion-corrosion performance of sphere-shaped morphology of nickel matrix nanocomposite strengthened with reduced graphene oxide nanoplatelets. Diam Relat Mater 104: 107763.
8. Akhtar S, Rehman S, Almessiere MA, Khan FA (2019) Synthesis of Mn0.5Zn0.5SmxEuxFe1.8−2xO4 Nanoparticles via the Hydrothermal Approach Induced Anti-Cancer and Anti-Bacterial Activities. J Nanomater 11: 1635.
9. Tombuloglu H, Slimani Y, Tombuloglu G, Almessiere M (2019) Tracking of NiFe2O4 nanoparticles in barley (Hordeum vulgare L.) and their impact on plant growth, biomass, pigmentation, catalase activity, and mineral uptake. Environ Nanotechnol Monit Manag 11: 100223.
10. Manikandan A, Yogasundari M, Thanrasu K, Dinesh A, Raja KK, et al. (2020) Structural, morphological and optical properties of multifunctional magnetic-luminescent ZnO@Fe3O4 nanocomposite. Phys E Low-Dimensional Syst Nanostructures 124: 114291.
11. Pubby K, Meena SS, Yusuf SM, Bindra SN (2018) Cobalt substituted nickel ferrites via Pechini's sol-gel citrate route: X-band electromagnetic characterization. J Magn Magn Mater 466: 430-445.
12. Srinivas Ch, Tirupanyam B V, Meena SS, Yusuf SM, Babu SCh, et al. (2016) Structural and magnetic characterization of co-precipitated NixZn1-xFe2O4 ferrite nanoparticles. J Magn Magn Mater 407: 135-141.
13. Gawas SG, Meena SS, Yusuf SM, Verenkar VMS (2016) Anisotropy and domain state dependent enhancement of single domain ferrimagnetism in cobalt substituted Ni-Zn ferrites†. New J Chem 40: 9275.
14. Banerjee AM, Pai MR, Meena SS, Tripathi AK, Bharadwaj SR (2011) Catalytic activities of cobalt, nickel and copper ferrospinels for sulfuric acid decomposition: The high temperature step in the sulfur based thermochemical water splitting cycles. Int J Hydrogen Energy 36: 4768-4780.
15. Sundararajan M, Kennedy LJ, Aruldoss U, Khadeer S, Vijaya JJ, et al. (2015) Microwave combustion synthesis of zinc substituted nanocrystalline spinel cobalt ferrite: Structural and magnetic studies. Mater Sci Semicond Process 40: 1-10.
16. Sundararajan M, Kennedy LJ, Vijaya JJ, Aruldoss U (2014) Microwave combustion synthesis of Co1−xZnxFe2O4 ($0 \leqslant x \leqslant 0.5$): Structural, magnetic, optical and vibrational spectroscopic studies. Spectrochim Acta Part A Mol Biomol Spectrosc 4: 421-430.
17. Sundararajan M, Sailaja V, Kennedy LJ, Vijaya JJ (2017) Photocatalytic degradation of rhodamine B under visible light using nanostructured zinc doped cobalt ferrite: Kinetics and mechanism. Ceram Int 43: 540-548.
18. Sundararajan M, Kennedy LJ (2017) Photocatalytic removal of rhodamine B under irradiation of visible light using Co1−xCuxFe2O4 ($0 \leq x \leq 0.5$) nanoparticles. Biochem Pharmacol 4: 4075-4092.
19. Manikandan A, Vijaya JJ, Sundararajan M, Meganathan C, Kennedy LJ, et al. (2013) Optical and magnetic properties of Mg-doped ZnFe2O4 nanoparticles prepared by rapid microwave combustion method. Superlattices Microstruct 64: 118-131.
20. Akhtar S, Ercan I, Belenli I (2019) Effect of bimetallic (Ca, Mg) substitution on magneto-optical properties of NiFe2O4 nanoparticles. Ceram Int 45: 6021-6029.
21. Salem BMK, Slimani Y, Hannachi E, Azzouz BF, Salem BM (2018) Bi-based superconductors prepared with addition of CoFe2O4 for the design of a magnetic probe. Cryogenics (Guildf) 89: 53-57.
22. Slimani Y, Unal B, Hannachi E, Selmi A, Almessiere MA, et al. (2019) Frequency and dc bias voltage dependent dielectric properties and electrical conductivity of BaTiO3single bondSrTiO3/(SiO2) x nanocomposites. Ceram Int 45: 11989-12000.
23. Slimani Y, Almessiere MA, Hannachi E, Mumta M, Manikandan A, et al. (2019) Improvement of flux pinning ability by tungsten oxide nanoparticles added in YBa2Cu3Oy superconductor. Ceram Int 45: 6828-6835.
24. Seevakan K, Manikandan A, Devendran P, Slimani Y, Baykal A, et al. (2019) Structural, magnetic and electrochemical characterizations of Bi2Mo2O9 nanoparticle for supercapacitor application. J Magn Magn Mater 486: 165254.

25. Slimani Y, Selmi A, Hannachi E, Almessiere MA, Mumtaz M, et al. (2019) Study of tungsten oxide effect on the performance of BaTiO3 ceramics. J Mater Sci Mater Electron 30: 13509-13518.

26. Slimani Y, Almessiere MA, Shirsath SA, Hannachi E, Yasin G, et al. (2020) Investigation of structural, morphological, optical, magnetic and dielectric properties of (1-x) BaTiO3/xSr0.92Ca0.04Mg0.04Fe12O19 composites. J Magn Magn Mater 510: 166933.

27. Slimani Y, Unal B, Almessiere MA, Hannachi E, Yasin G, et al. (2020) Role of WO3 nanoparticles in electrical and dielectric properties of BaTiO3-SrTiO3 ceramics. J Mater Sci Mater Electron 31: 7786-7797.

28. Qian H, Li J, Sun L, Chen W, Sheng GD, et al. (2009) Combined effect of copper and cadmium on Chlorella vulgaris growth and photosynthesis-related gene transcription. Aquat Toxicol 94: 56-61.

29. Hannachi E, Slimani Y, Azzouz BF, Ekicibil A (2018) Higher intra-granular and inter-granular performances of YBCO superconductor with TiO2 nano-sized particles addition. Ceram Int 44: 18836-18843.

30. Slimani Y, Selmi A, Hannachi E, Almessiere MA, Baykal A, et al. (2019) Impact of ZnO addition on structural, morphological, optical, dielectric and electrical performances of BaTiO3 ceramics. J Mater Sci Mater Electron 30: 9520-9530.

31. Almessiere MA, Slimani Y, Baykal A (2018) Exchange spring magnetic behavior of Sr0.3Ba0.4Pb0.3Fe12O19/(CuFe2O4) x nanocomposites fabricated by a one-pot citrate sol-gel combustion method. J Alloys Compd 762: 389-397.

32. Slimani Y, Almessiere MA, Korkmaz AD, Guner S, Güngüne H, et al. (2019) Ni0.4Cu0.2Zn0.4TbxFe2-xO4 nanospinel ferrites: Ultrasonic synthesis and physical properties. Ultrason Sonochem 59: 104757.

33. Slimani Y, Almessiere MA, Sertkol M, Shirsath SE, Baykal A, et al. (2019) Structural, magnetic, optical properties and cation distribution of nanosized Ni0.3Cu0.3Zn0.4TmxFe2−xO4 ($0.0 \leq x \leq 0.10$) spinel ferrites synthesized by ultrasound irradiation. Ultrason Sonochem 57: 203-211.

34. Slimani Y, Almessiere MA, Güner S, Kurtan U, Sagar E, et al. (2020) Magnetic and microstructural features of Dy3+ substituted NiFe2O4 nanoparticles derived by sol-gel approach. J Sol-Gel Sci Technol 95: 202-210.

35. Nalwa Hari (2001) Nanostructured materials and nanotechnology: Concise edition. Elsevier pp: 834.

36. Muyssen BT, Janssen CR (2001) Zinc acclimation and its effect on the zinc tolerance of Raphidocelis subcapitata and Chlorella vulgaris in laboratory experiments. Chemosphere 45(4-5): 507-514.

37. Chauhan L, Shukla A K, Sreenivas K (2015) Dielectric and magnetic properties of Nickel ferrite ceramics using crystalline powders derived from DL alanine fuel in sol-gel auto-combustion. Ceram Int 41: 8341-8351.

38. Ortiz-quin J, Pal U, Villanueva MS (2018) Structural, Magnetic, and Catalytic Evaluation of Spinel Co, Ni, and Co-Ni Ferrite Nanoparticles Fabricated by Low-Temperature Solution Combustion Process. ACS omega 3(11): 14986-15001.

39. Joshi S, Kumar M, Chhoker S, Srivastava G, Jewariya M, et al. (2014) Structural, magnetic, dielectric and optical properties of nickel ferrite nanoparticles synthesized by co-precipitation method. J Mol Struct 1076: 55-62.

40. Dhiwahar AT, Maruthamuthu S, Marnadu R, Sundararajan M, Manthrammel MA, et al. (2021) Improved photocatalytic degradation of rhodamine B under visible light and magnetic properties using microwave combustion grown Ni doped copper ferrite spinel nanoparticles. Solid State Sci 113: 106542.

41. Baskar S, Yuvaraj S, Sundararajan M (2020) J Supercond Nov Magn 33: 3949.

42. Baskar S, Partha YS, Subudhi S, Dash CS (2020) Influence of Sr2+ ion substitution on structural, morphological, optical, thermal, and magnetic behavior of MgFe2O4 cubic spinel. J Chin Chem Soc 68: 630-638.

43. Kagdi AR, Solanki NP, Carvalho FE, Meena SS, Pullar RC, et al. (2018) Influence of Mg substitution on structural, magnetic and dielectric properties of X-type bariumsingle bondzinc hexaferrites Ba2Zn2-xMgxFe28O46. J Alloy Compd 741: 377-391.

44. Kombaiah K, Vijaya JJ, Kennedy LJ, Kaviyarasu K, (2019) Catalytic studies of NiFe2O4 nanoparticles prepared by conventional and microwave combustion method. Mater Chem Phys 221: 11-28.

45. Chavan P, Naik LR (2017) Investigation of energy band gap and conduction mechanism of magnesium substituted nickel ferrite nanoparticles. Phys Status Solidi 214(9): 1700077.

46. Baykal A (2019) Ultrason Sonochem 58: 104654.

47. Shirsath SE, Ercan I, Ozçelik B (2019) Sonochemical synthesis of Eu3+ substituted CoFe2O4 nanoparticles and their structural, optical and magnetic properties. Ultrason Sonochem 58: 104621.

48. Almessiere MA, Slimani Y, Korkmaz AD, Güner S, Baykal A, et al. (2020) Sonochemical synthesis of Dy3+ substituted Mn0.5Zn0.5Fe2-xO4 nanoparticles:

Structural, magnetic and optical characterizations. Ultrason Sonochem 61: 104836.

49. Li M, Hu C, Zhu Q, Chen L, Kong Z, et al. (2006) Copper and zinc induction of lipid peroxidation and effects on antioxidant enzyme activities in the microalga Pavlova viridis (Prymnesiophyceae). Chemosphere 62: 565-572.

50. Tomitaka A, Hirukawa A, Yamada T, Morishita S, Takemura Y (2009) Biocompatibility of various ferrite nanoparticles evaluated by in vitro cytotoxicity assays using HeLa cells. J Magn Magn Mater 321: 1482.

51. Sagadevan S, Chowdhury ZZ, Rafique RF, Brunswick N (2018) Preparation and Characterization of Nickel ferrite Nanoparticles via Co-precipitation Method. Mater Res 21: 21.

52. Cristina A, Andronic L (2021) Aquatic Toxicity of Photocatalyst Nanoparticles to Green Microalgae *Chlorella vulgaris*. Water 1: 77.

53. Halbus AF, Horozov TS, Paunov VN (2020) Surface-Modified Zinc Oxide Nanoparticles for Antialgal and Antiyeast Applications. ACS Appl Nano Mater 1: 440.

54. Millington LA, Goulding KH, Adams N (1988) The influence of growth medium composition on the toxicity of chemicals to algae. Water Res 22: 1593.